A Sense of Touch for the Shadow Modular Grasper

Nicholas Pestell[1], Luke Cramphorn[1], Fotios Papadopoulos[2] and Nathan F. Lepora[1]

***Abstract*—In this study, we have designed and built a set of tactile fingertips for integration with a commercial, three-fingered robot hand, the Shadow Modular Grasper. The fingertips are an evolution of an established optical, biomimetic tactile sensor, the TacTip. In developing the tactile fingertips, we have progressed the technology in areas such as miniaturization, development of custom-shaped finger-pads and integration of multiple sensors. From these fingertips, we extract a set of high-level features with intuitive relationships to tactile quantities such as contact location and pressure. We present a simple linear-regression method for predicting roll and pitch of the finger-pad relative to a surface normal and show that the method generalises to unknown depths and shapes. Finally, we apply this prediction to a grasp-control method with the Modular Grasper and show that it can adjust the grasp on three real-world objects from the YCB object set in order to attain a greater area of contact at each fingertip.**

***Index Terms*—Force and Tactile Sensing; Grasping; Perception for Grasping and Manipulation; Biomimetics**

I. Introduction

ROBOT hands have seen accelerated development in recent years [1], advancing attributes such as dexterity, grip strength and ease of use. Two-fingered grippers are deployed in large numbers for repetitive manufacturing tasks, whereas, more advanced, multi-fingered hands are yet to find applications outside of research. Thus, a gap persists for automation of small scale production, where robots are required to grasp and manipulate unknown objects [2]. This gap can only be filled by dexterous, multi-fingered robot hands.

Given the advances in the state-of-the-art of robot hands, it is surprising such hands have not yet found widespread application. One contributing factor may be a lack of sufficient tactile sensing capabilities. Indeed, it is known that humans rely heavily on their sense of touch to maintain a stable grasp [3]. Whilst there have been many attempts at improving grasp stability with the introduction of tactile sensing, primarily with data-driven approaches [4]–[9], these methods are often impractical due to the large quantities of training data required and poor generalisability. In general, the tactile sensors are low resolution, array-based technologies, which do not allow for extraction of high-level features with a more direct relationship to the object being held.

Manuscript received: September, 10, 2018; Revised December, 6, 2018; Accepted February, 06, 1991.

This paper was recommended for publication by Editor Dan Popa upon evaluation of the Associate Editor and Reviewers' comments. This work was supported by an EPSRC IAA award on a 'Tactile smart grasping system'. NL was supported by a Leverhulme, Leadership Award on a 'A biomimetic forebrain for robot touch' (RL-2016-39).

[1]NP, LC and NL are with the Department of Engineering Mathematics and Bristol Robotics Laboratory, University of Bristol, Bristol, U.K. {n.pestell, ll14468, n.lepora}@bristol.ac.uk

[2]FP is with the Shadow Robot Company, London, U.K. fotios@shadowrobot.com

Digital Object Identifier (DOI): see top of this page.

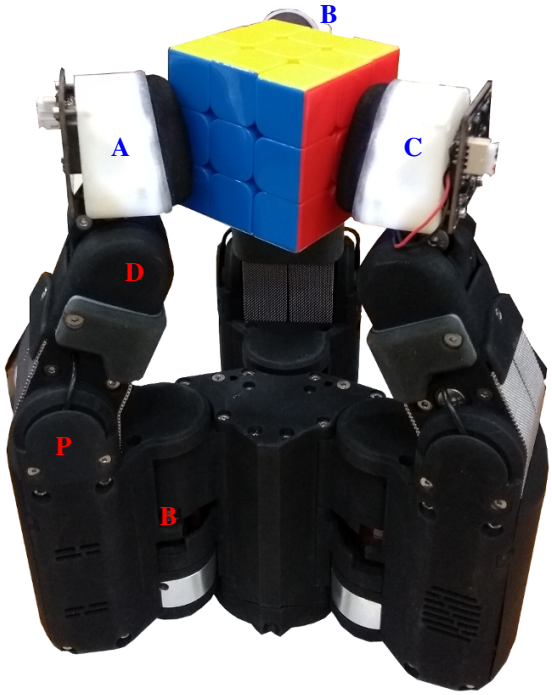

Fig. 1: Image of the developed tactile sensors integrated with the Shadow Modular Grasper. Base, proximal and distal joints are labelled in red, **B**, **P** and **D** respectively. Tactile fingertips **A**, **B** and **C** are labelled in blue.

This study presents the development of a high-definition, biomimetic tactile fingertip and its integration with a three-fingered, fully-actuated, robot hand: the Shadow Robot Company's Modular Grasper (Fig. 1).

We extract features from high-dimensional raw tactile images and infer information relevant to grasp quality using simple algorithms and relatively small amounts of training data in comparison to documented data-driven approaches. The overall aim is to develop a method for improving grasp quality, that could form part of a higher-level modular grasp control framework, in a way that is robust to variations such as object shape, orientation and weight.

II. Background and Related Work

A seminal study by Kawasaki et al. [10] in 2002 set a high benchmark for forthcoming work into endowing robot hands with a sense of touch. The authors presented a sophisticated, 16-DOF, anthropomorphic hand, the Gifu hand II. The hand was equipped with 624 resistive tactile pads distributed across all five fingers and the palm.

In 2011, Romano et al. [11] conducted an innovative study into a grasp control framework using touch as an integral component, using comparatively rudimentary hardware: two 5x3 capacitive tactile sensors and an accelerometer integrated with the PR2 two-fingered gripper. Different states within the control system were triggered by hard-coded tactile signals.

Since Romano's influential paper, many researchers have integrated tactile sensors with dexterous robot hands [4], [5], [7], [9], [12]–[14]. In contrast to the Romano's study, however, the trend has been towards data-driven methods:

In [4], an under-actuated, Robotiq gripper was equipped with 6 array-based pressure sensors. A kernel logistic regression model, trained with tactile data from 192 grasps, predicted grasp success to 89% accuracy. Similarly, in [5], two 7x4 capacitive tactile arrays were integrated on the finger-pads of a Robotiq two-fingered, griper. 1000 grasps trained a CNN to achieving a prediction accuracy of 88.4%.

The authors of [7] propose a method for re-grasp: a Barrett hand was equipped with array-based Biotac tactile sensors. Reinforcement learning was used to predict stable re-grasp of a single object, trained with a total of 50 hours of real robot data. Grasp success was improved from 42% to 97%.

The bias towards these data-driven methods is partially due to low resolution of the tactile sensors employed. Without sufficient acuity, sensors provide un-intuitive representations of tactile contact. In contrast, optical tactile sensors, e.g. the Gelsight [15] and the TacTip [16], provide high-resolution tactile images which ease interpretation.

The Gelsight was integrated with the Weiss WSG-50 gripper [9]. Deep CNNs predicted probability of successful re-grasp given a proposed action achieving a re-grasp success rate of 83.8% using vision and tactile. However, this method required a large data-set: 6,450 grasps on 65 objects.

Here our presented fingertip design is based on an established tactile sensing device: the TacTip [16], [17]. Originally developed in 2009, the TacTip is an optical tactile sensor with a biomimetic design based on human tactile sensing [18].

The TacTip has shown potential for integration with robot hands, e.g. [19] where a TacTip based tactile thumb (TacThumb) was integrated with the Open-Hand M2 gripper and [20] where two TacTip devices were mounted as fingertips on the Open-Hand GR2 gripper. In both of these studies, the authors utilise a supervised-learning method to achieve precise in-hand manipulation of custom-made objects.

Whilst the aforementioned literature shows clear benefits of tactile sensing for grasping, a common shortcoming is the nature of the tactile data available and/or the amount of data required to interpret it. Here we present a more flexible platform by integrating a highly sensitive, high-resolution, optical tactile sensor with a fully-actuated industrial robot hand. We demonstrate the potential for this system to improve grasps on unknown, real-world objects by presenting a method for grasp adjustment that could feasibly form part of a higher-level control framework.

III. Materials and Methods

A. Shadow Modular Grasper

The Shadow Modular Grasper is fully actuated with 9 degrees of freedom (three per finger). The system is fully integrated with ROS and the user can control both specific joints and whole-hand grasps. Each identical finger has base, proximal and distal joints with one DC motor per joint and can be easily attached and detached resulting in a modular system. The full hand has a total mass of 2.7 kg and a payload of 2 kg and each finger can apply 10 N of normal force. Each joint has a dedicated torque sensor for closed loop control and also features a back-drivable gearbox enabling inherent compliance, which is an essential component when working in unstructured environments. The whole unit requires only two connections: power and comms (EtherCAT) [21].

B. Tactile Sensing

1) Tactile Fingertip Design: Tactile sensing is enabled by replacing the fingertips of the Modular Grasper with three custom-built tactile sensors (Fig. 1). The fingertips are comprised of two main components: a compliant finger-pad which deforms when contacted and a rigid body which fixes the camera in place and houses other electronics (Fig. 2).

The finger-pad is fully 3D-printed as a single part with a multi-material 3D-printer (Stratasys Objet). A sensing surface 'skin' is printed in Tango Black+ (Shore A 26-28). The inside of the skin is tessellated with a triangular pattern of 97 pins (Tango Black+, 3 mm length and 2 mm diameter). White markers on the end of pins are printed in rigid Vero White and provide a visual representation of the tactile stimulation. A rim (Vero White) enables a press-fit connection to the fingertip body. A clear acrylic sheet (2 mm thick) is glued into the rim resulting in a small cavity between the skin and the acrylic lens. This cavity is filled with a two-part cure, clear, silicone gel (RTV27905, Techsil UK (∼Shore OO 10)) using a manual injection method. The gel helps to reduce hysteresis while still enabling deformation.

The finger-pad is press-fit into a hollow body which is 3D-printed in ABS. A 2.0 megapixel CMOS array USB web-cam (ELP cameras) is mounted on the back via four M2 screws. The camera is used in HD mode (1920x1080). Dimensions of the fingertip body are optimized to enable a view of all markers whilst minimizing the overall depth of the fingertip. The markers are illuminated by four LEDs arranged on two PCB strips of two LEDs each. The PCBs are glued to the inside of the body, close to the interface with the finger-pad.

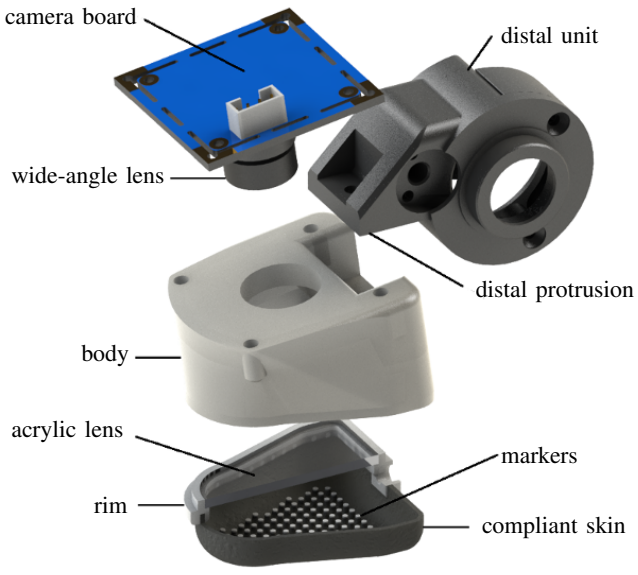

Fig. 2: Exploded CAD model of the tactile fingertip.

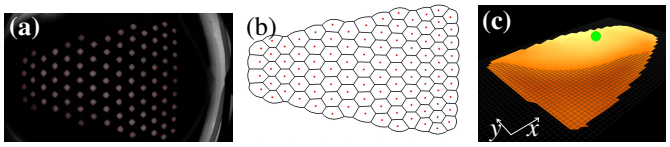

Fig. 3: **(a)**: View of markers imaged by the camera and tracked with OpenCV. **(b)**: Voronoi tessellation over markers. **(c)**: Visual representation of surface deformations with centre-of-pressure shown as a green spot.

The final system employs a wide-angle lens (2.1 mm focal length, 150° view angle), which enables focused images of the full marker array (Fig. 3a).

2) Hardware Integration: Integration of three sensors has, to date, not been attempted with TacTip-based sensing. A solution proposed here is to connect each tactile fingertip to its own dedicated USB-hub. With three dedicated hubs, the data transfer occurs in parallel without reducing the frame rates, ∼20 fps per camera.

3) Tactile Feature Extraction: Feature extraction is performed using a Voronoi method previously demonstrated to achieve direct inference of pressure and contact locations with the TacTip [22]. Marker positions are tracked with a simple blob detection algorithm implemented with OpenCV in Python. A Voronoi tessellation is created over the sensor skin, treating the marker positions as seeds (Python, SciPy) (Figs. 3a and b). The areas of each Voronoi cell are related to local skin deformation, where increased size corresponds to indentation and hence pressure.

Visual representations of the surface deformation are obtained by interpolating the change in Voronoi cell areas over the fingertip. A centre-of-pressure, a tactile analogue of centre-of-mass, is computed as an average of marker positions weighted by their corresponding cell area (Fig. 3c).

C. Off-line Testing - methods

Orientation of the fingertip relative to the contact surface may be of importance when grasping an object. For example, greater frictional forces are achieved with a larger contacting surface area, which is affected by relative angle between fingertip and object. Here we examine the ability of the presented sensor and described feature extraction technique for perceiving roll and pitch relative to a flat surface.

1) Data collection: The fingertip is mounted as an end-effector on a six degree-of-freedom robot arm (UR5, Universal Robotics). The sensor maintains continual contact with a flat acrylic plate and the robot re-orients the sensor relative to the plate. Data is sampled randomly from a 2D grid of roll, ϕ, and pitch, θ, values, $-16^\circ \leq \phi \leq 16^\circ$ and $-11^\circ \leq \theta \leq 3^\circ$.

Experimental set-up is shown in Fig. 4. ϕ and θ angles are equally space by 2° and 1° respectively yielding, a total of $N_\phi N_\theta = 17 \times 15 = 255$ data points.

Three seconds of training data (~ 60 frames) are collected for each sample. A sample consists of a time series of centre-of-pressure vales r_{ki}, where $1 \leq k \leq N_{\text{frames}}$ and $1 \leq i \leq N_{\text{dims}}$; $N_{\text{frames}} \simeq 60$ and $N_{\text{dims}} = 2$ for x and y positions.

Three separate test sets are collected, on the same acrylic plate, of 200 data points each, sampled at random from a continuous space within the same range of ϕ and θ. Each set is collected at a different depth since we are interested the degree to which our methods are pressure invariant. The depths, -0.5 mm $\leq z_l \leq$ 0.5 mm, are equally spaced, where $z_l = 0$ mm corresponds to the depth used for training.

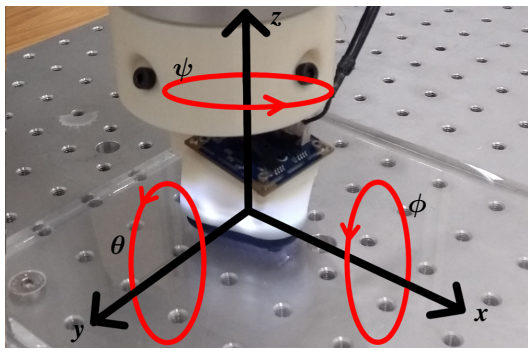

Fig. 4: Data collection set-up with tactile fingertip mounted as an end-effector on a UR5 robot arm. Showing roll, ϕ, pitch, θ and yaw, ψ orientations relative to the sensor.

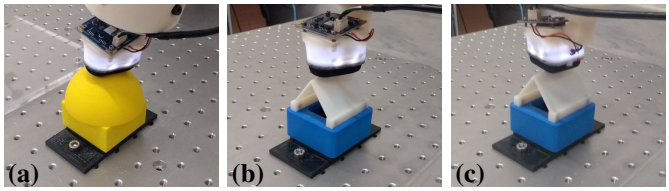

Fig. 5: **(a)**: Data being collected on the dome stimulus. **(b)** and **(c)**: Data being collected on the edge stimulus at ψ = 0 and 90° respectively.

The ranges of ϕ and θ and of z are chosen in combination, to avoid damage to the sensor but also provide examples extremely light touch: pressure on the sensor is maximised when ϕ and θ are at extremes and z is minimised. The location of ϕ and θ ranges additionally provide a contact area which is maximised when both ϕ and θ = 0.

To further examine the generalisability of our method we perform additional tests with data collected on two generic 3D-printed shapes: a dome and an edge. On the edge, we collect two sets with different yaw, ψ, angles: 0 and 90° respectively (Fig. 5). Data is collected using the same random sampling procedure as with the acrylic plate.

We repeat the training and testing data collection procedures once for each fingertip. This is because of small inconsistencies in the manufacturing procedure which may lead to different physical and optical responses.

2) Perception: Prior to training, data is averaged across frames, so each sample has $N_{\text{dims}} = 2$ features. We map centre-of-pressure-xy position to ϕ and θ via three separate multivariate, linear models: A simple linear model (1st-order polynomial), 2nd- and 3rd-order polynomials.

D. System Integration - On-line Grasp Adjustment

For the purpose of this study, we intend to use the predicted ϕ and θ (Section III-C) to adjust a grasp. Three Python drivers, one for each sensor, run on the host PC and interact with the grasp controller (C++) via a ROS-network.

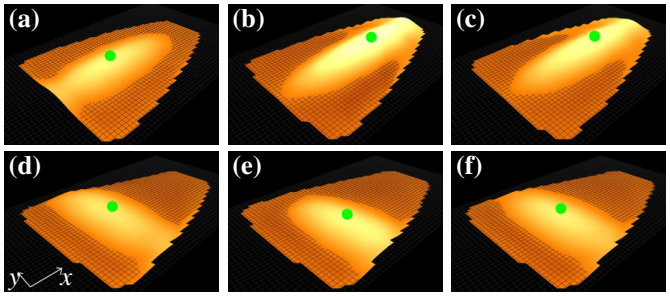

Fig. 6: **(a)**, **(b)** and **(c)**: Visualisations of surface deformation with different values of ϕ and θ with $\psi = 0°$. **(d)**, **(e)** and **(f)**: Visualisations of surface deformation with different values of ϕ and θ with $\psi = 90°$.

The high-level strategy consists of independent control of each joint through its dedicated motor (full actuation). Each joint can be controlled in either position or torque mode. A grasp is comprised of two distinct phases: *(i)* closing phase and *(ii)* adjustment phase. These two phases are implemented within an update loop running at 1 kHz which iteratively updates joint modes and targets according to sensor data.

i) During the closing phase all joints are controlled in position mode and commanded to a set of target angles via a PID which is an implementation of the roscontrol ROS-package. Throughout this phase, the hand controller is listening to a set of 'contact-detection' ROS-topics, published by each driver. Contact is determined by upward threshold crossing on the surface deformation (Fig. 3). Upon contact-detection each respective finger stops moving.

ii) After all sensors have detected contact the adjustment phase is entered: the controller switches all proximal joints to torque mode and applies a fixed squeezing torque to the object. Base and distal joints remain in position mode and are servoed with the PID controller used in phase *i)*. PID inputs are ϕ and θ predictions for base and distal joints respectively, thus, the hand attempts to servo the finger-pads to ϕ and $\theta = 0$. To steady the grasp, this adjustment phase has a time-out period, the length of which, is obtained from experimentation (Section IV-B). see Fig. 1 for reference of joint names.

IV. Results

A. Off-line Testing - results

We compared three competing model types (simple, 2nd- and 3rd-order linear models) for predicting ϕ and θ (Section III-C). Our model should accurately approximate training data whilst generalising to unobserved samples. Table I shows R^2 scores for three competing models for all three tips, on test data collected on the acrylic plate at each test depth (see Fig. 4), the dome and on the edge at $\psi = 0$ and $90°$ (see Fig. 5).

On the flat plate, where test sets were collected at training depth (0 mm), the 3rd-order polynomial model achieved the highest R^2 scores over the whole set (0.95, 0.94, and 0.93). This model, however, under-performed at the two unseen depths, particularly at 0.5 mm where it achieved the lowest three R^2 scores for the flat stimulus (0.67, 0.28 and 0.40).

In contrast, both 1st- and 2nd-order polynomials performed more consistently on the flat plate: The lowest R^2 scores

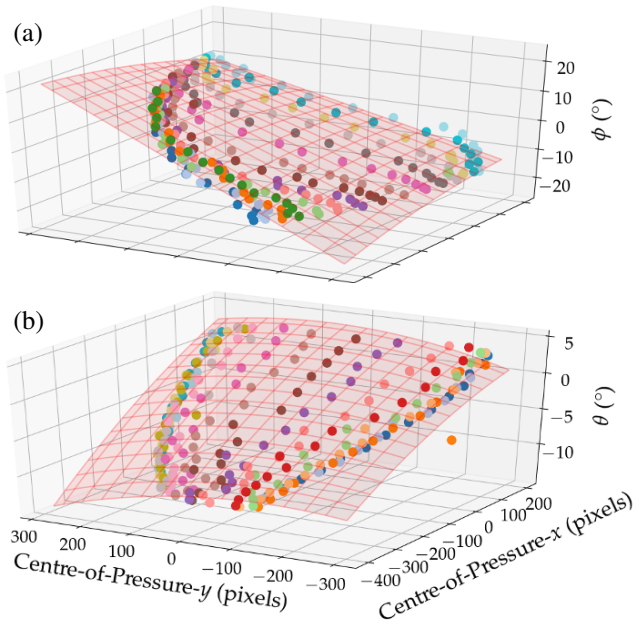

Fig. 7: **(a)**: Scatter plot of xy-centre-of-pressure vs ϕ. **(b)**: Scatter plot of xy-centre-of-pressure vs θ angle. In both plots, the surface shows a 2nd degree polynomial fit and each colour represents a constant θ and ϕ in **(a)** and **(b)** respectively.

were 0.72 and 0.71 for the 1st- and 2nd-order polynomials respectively. This improved consistency is likely due to a lower variance in the models, giving better generalisation.

All three models are capable of generalising to the dome stimulus: all R^2 scores are above 0.6. As with the unobserved depths, the worst performing model was the 3rd order polynomial scoring 0.75 averaged across the three tips, vs. 0.88 and 0.86 for 1st- and 2nd-order polynomials respectively.

All three models, however, performed poorly on the edge at both ψ angle orientations: the highest R^2 score was 0.46. We believe this is caused by a singularity when exposed to edge like stimuli: the centre-of-pressure remains fixed in the dimension perpendicular to the edge regardless of ϕ and θ. Fig. 6 demonstrates this effect. The centre-of-pressure remains consistent in the x dimension when $\psi = 0°$ and, contrastingly, it remains consistent in the y dimension when $\psi = 90°$ regardless of ϕ and θ in both cases.

To test this hypothesis we examined R^2 scores attained when making separate predictions of ϕ and θ for data collected on the edge. Results of this test are shown in Table II. The three models perform well at $\psi = 0°$ when predicting θ but poorly when predicting ϕ. At $\psi = 90°$, good performance is achieved for ϕ predictions whereas the models perform poorly when predicting θ. In both cases, $\psi = 0°$ and $90°$, better performance is observed when predicting the dimension which is parallel to the edge orientation, confirming the singularity hypothesis. We have, therefore, identified a limitation with sensing under these conditions.

Based on results from this data, we consider the 2nd-order model to be the most suitable for predicting ϕ and θ with the application to robot hands.

Visualisations of the 2nd-order polynomial model for tip-B

TABLE I: R^2 scores for 1st-, 2nd- and 3rd-order polynomial linear regression for tips A, B and C, as labelled in Fig. 1, calculated for test sets on the flat acrylic plate at depths of -0.5, 0 and 0.5 mm, the dome and the edge at ψ = 0 and 90°.

	1st order						**2nd order**						**3rd order**					
Stimulus	**Flat plate**			**Dome**	**Edge**		**Flat plate**			**Dome**	**Edge**		**Flat plate**			**Dome**	**Edge**	
Depth (mm)	**-0.5**	**0**	**0.5**	**0**	**0**		**-0.5**	**0**	**0.5**	**0**	**0**		**-0.5**	**0**	**0.5**	**0**	**0**	
ψ (°)	**0**	**0**	**0**	**0**	**0**	**90**	**0**	**0**	**0**	**0**	**0**	**90**	**0**	**0**	**0**	**0**	**0**	**90**
tip-A	0.91	0.90	0.91	0.92	0.42	-0.01	0.92	0.91	0.92	0.90	0.46	-0.07	0.84	0.95	0.67	0.82	0.28	-0.03
tip-B	0.87	0.89	0.72	0.87	0.42	0.25	0.89	0.92	0.71	0.87	0.46	0.29	0.85	0.94	0.28	0.83	0.32	0.29
tip-C	0.88	0.88	0.81	0.84	0.36	0.17	0.90	0.90	0.82	0.80	0.36	0.21	0.76	0.93	0.40	0.61	0.21	0.25

TABLE II: R^2 scores for separate predictions of ϕ and θ for 1st- (simple), 2nd- and 3rd-order polynomial linear regression for tips A, B and C, as labelled in Fig. 1, calculated for test sets collected on the edge stimulus at ψ of 0 and 90°.

	1st order				**2nd order**				**3rd order**			
ψ (°)	**0**		**90**		**0**		**90**		**0**		**90**	
target	ϕ	θ	ϕ	θ	ϕ	θ	ϕ	θ	ϕ	θ	ϕ	θ
tip-A	0.33	0.89	0.88	-3.7	0.37	0.92	0.80	-3.7	0.18	0.78	0.76	-3.3
tip-B	0.32	0.87	0.84	-2.5	0.35	0.91	0.86	-2.4	0.23	0.77	0.89	-2.5
tip-C	0.25	0.91	0.96	-4.2	0.25	0.91	0.84	-3.2	0.11	0.70	0.92	-3.4

are shown in Fig. 7. The data is well ordered and the model appears a suitable fit. We observe strong correlations of centre-of-pressure-x and -y positions with θ and ϕ respectively. This is expected since the x- and y-axis align with θ and ϕ respectively. We also observe some correlation of centre-of-pressure-y and -x positions with and θ and ϕ respectively, suggesting both features are useful predictors.

B. On-line Grasp Adjustment

Here we investigate the capabilities of the integrated Shadow Modular Grasper with tactile fingertips. We look at the capacity for perceived ϕ and θ to be used in a grasp adjustment procedure (Section III-D) and the potential for this to improve grasp quality on three objects from the YCB object set: A Rubik's cube, Pringles can and mustard bottle. Informed by results in Section IV-A, ϕ and θ are predicted using a 2nd-order polynomial regression model.

We have provided a supplementary video containing a range of grasp attempts on all three objects. Within these are examples of successful and unsuccessful grasps.

Fig. 8 shows successful grasps of all three objects. Alongside each image are tactile visualisations from each fingertip. The objects are initially held in place by a human participant before passing over to the robot when all three fingers have made contact. The top row shows images at initial contact detection (prior to tactile adjustment) and the bottom row shows images after tactile adjustment, ∼10 s later.

The top and bottom rows of Fig. 8 show noticeable differences in both the grasp images and the tactile visualisations. In general, the grasp images show that the fingertips rotated around each object to minimise ϕ and θ. Inspection of the tactile visualisations suggests that overall deformation of each fingertip increased subsequent to adjustments in all cases. This suggests that, for these examples, the grasp controller performed as designed: to increase contact surface area and, thus, also the frictional forces at each fingertip.

The hand made a good initial grasp of the Pringles can owing to its symmetrical shape, with ϕ close to zero prior to adjustment for all three fingertips. We observe a slight modification of θ for each fingertip which in-turn increased the contact surface area. The mustard bottle is the most irregular of the three presented objects. Despite this, the hand maintained a stable grasp throughout the adjustment phase and, increased the contact surface area on all three fingertips.

On the Rubik's cube, all three fingertips contacted edges resulting in singularities for predicting ϕ (Section IV-A). However, all three fingers moved to settle the centre-of-pressure in the middle of each finger-pad. For fingertips A and C we believe this is because initially the centre-of-pressure was towards the edge of the pad: despite this producing a measurement singularity, our algorithm perceives an off-set in ϕ, so the base joint is servoed to counteract this, thus rolling the sensor onto the face of the Rubik's cube. Contrastingly, fingertip B maintained its location on the edge of the cube which we consider to again be a consequence of the perceived ϕ. The initial centre-of-pressure was near the middle of the finger-pad, so our algorithm perceived ϕ to be small. Whilst this grasp may not maximise the overall contact surface area, it is a stable configuration given its starting point.

Fig. 9 shows base and distal joint angles and centre-of-pressure-x and -y positions vs. time when successfully grasping the Rubik's cube, for fingers A, B and C, (as labelled in Fig. 8). All three fingers detect contact at roughly the same time. Subsequently, joint angles are adjusted before reaching the time-out, observed as a flattening of the blue curves. A time-out of 10 s appears to give the hand suitable time to re-adjust. During the same period, the centre-of-pressure migrates towards 0 in both dimensions. The shapes of these curves suggest that hand control performed as designed: to servo base and distal joints in order to shif the centre-of-pressure to the middle of each finger-pad.

In the case of unsuccessful grasps (please see supplementary video), the hand typically 'spills' the object. We attribute this to an 'over-adjustment'. The hand initially grasps the object with horizontal forces balanced across all fingertips. Joints are then adjusted. At some point, prior to time-out, adjustment moves the hand beyond a stable configuration, i.e. normal forces exerted by each fingertip become sufficiently un-balanced to push the object out of a grasp.

V. DISCUSSION

This work is entirely novel in its approach to on-line grasp adjustment. That is, using tactile sensing to predict the angle of contact and adjust hand orientation accordingly, thus maximising the area of contact at each fingertip. Furthermore, this is the first study into the use of optical biomimetic tactile sensors with multi-fingered robot hands.

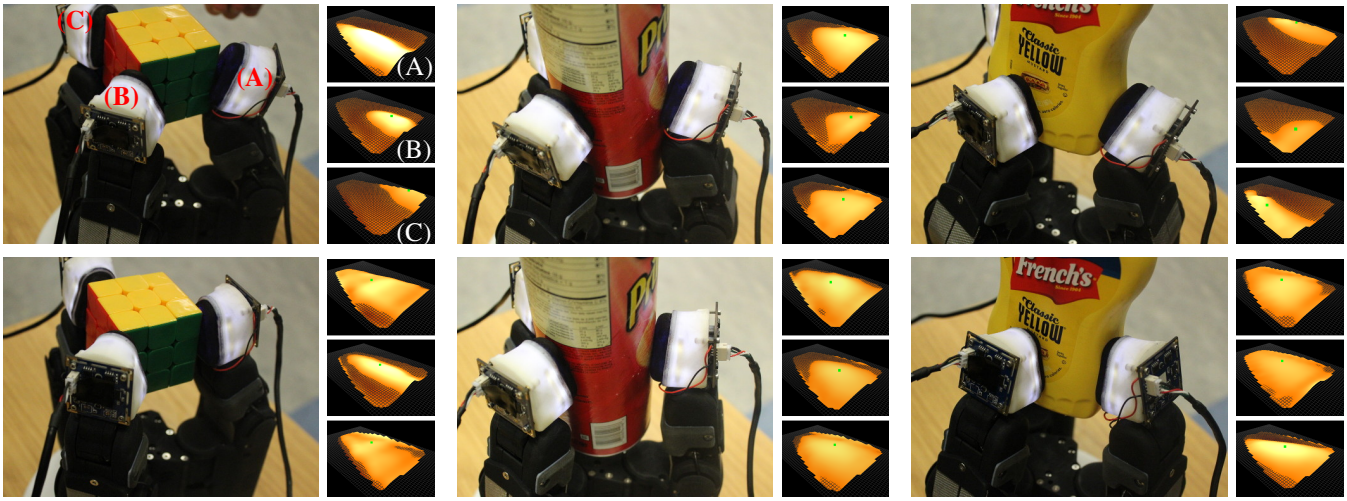

Fig. 8: Images of the grasps on the Rubik's cube, Pringles can and mustard bottle, before and after tactile adjustment; top and bottom rows respectively. Tactile visualisations for the three fingertips are displayed to the right of each grasp image. Fingertips are labelled on the top left image and visualisations for reference.

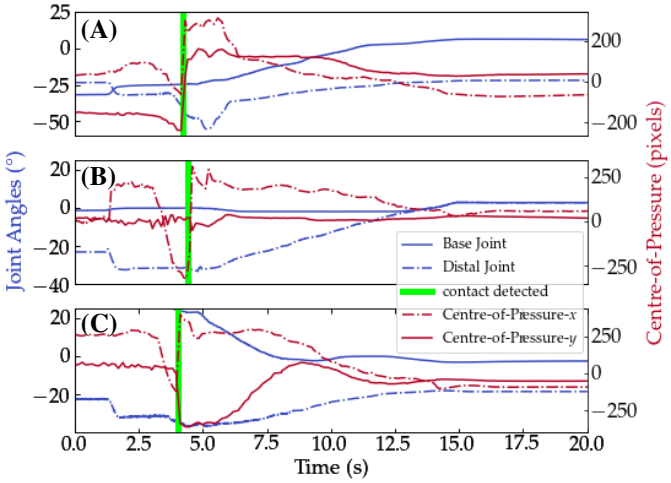

Fig. 9: Plots of base and distal joint angles (blue) and *xy* centre-of-pressure (red) versus time, for fingers A, B and C, whilst grasping the Rubik's cube. Vertical green lines show when each finger detected contact.

A 2nd-order polynomial model was identified as a suitable method for predicting ϕ and θ due to a balance of accuracy and generalisation. A clear limitation was encountered where a singularity was observed for predicting orientations when sensing perpendicular to the edge. This constraint is not limited to the presented hardware or method since it is produced by a physical singularity observed in the raw tactile signal.

The designed system was able to successfully grasp and hold a Rubik's cube, Pringles can and mustard bottle. The adjustment mechanism behaved as designed: to obtain a greater surface area of contact and a more centrally located pressure, both of which are likely to improve grasp quality.

A limitation in terms of robustness was exposed: roughly half the trails were able to maintain a stable grasp throughout the entire adjustment phase, whilst the remaining trails resulted in the object being 'spilled'. The primary cause of failure was 'over-adjustment' resulting in the forces becoming unbalanced between the fingers.

Recently, OpenAI achieved in-hand manipulation with impressive levels of dexterity using deep reinforcement learning [23]. To aid training, simulation was used, however, this is a challenge for touch, hence, this modality was omitted from their research. This highlights a need for learning-free approaches to using touch for application with any hand, without the need for re-training or simulation.

A key benefit of the developed approach for using touch is that, whilst it requires high-resolution tactile sensing, it can be easily applied to any robotic hand with the required degrees of freedom. This is owing to the intuitive output from the sensors (roll and pitch angle) which can be directly applied to joint angles of the gripper. As a consequence no prior training with the robot hand is required.

VI. Conclusions and Future Work

In this study, we presented the integration of an established optical tactile sensing technology, the TacTip, with a three-fingered, commercial robot hand: the Shadow Modular Grasper. The sensors were tested for predicting roll and pitch relative to a flat surface and two generic shapes: a dome and an edge. Finally, we integrated tactile output with the hand control and demonstrated a novel approach to real-time grasp adjustment, using predicted roll and pitch angles to adjust the grasp on three real-world objects for attaining greater contact surface areas at each finger-pad.

Robustness was identified as an area to improve upon in further iterations. We believe tuning the time-out period may help to provide robustness by reducing the chance of over-adjustment. A suitable time out period could be learned for each object and adjusted autonomously.

The system developed in this paper could be integrated into a high-level, modular controller, similar to the approach taken by Romano et al. [11]. We would like to autonomously and repeatedly grasp and set down a number of real-world objects. This could be achieved by mounting the hand on an arm and using vision to locate objects in the work space. In this way, a quantitative measure of performance could be attained.

REFERENCES

[1] Z. Xu and E. Todorov, "Design of a highly biomimetic anthropomorphic robotic hand towards artificial limb regeneration," in *2016 IEEE International Conference on Robotics and Automation (ICRA)*, May 2016, pp. 3485–3492.

[2] Z. Kappassov, J.-A. Corrales, and V. Perdereau, "Tactile sensing in dexterous robot hands — review," *Robotics and Autonomous Systems*, vol. 74, pp. 195 – 220, 2015. [Online]. Available: http://www.sciencedirect.com/science/article/pii/S0921889015001621

[3] R. S. Johansson and G. Westling, "Roles of glabrous skin receptors and sensorimotor memory in automatic control of precision grip when lifting rougher or more slippery objects," *Experimental Brain Research*, vol. 56, no. 3, pp. 550–564, Oct 1984. [Online]. Available: https://doi.org/10.1007/BF00237997

[4] E. Hyttinen, D. Kragic, and R. Detry, "Learning the tactile signatures of prototypical object parts for robust part-based grasping of novel objects," in *2015 IEEE International Conference on Robotics and Automation (ICRA)*, May 2015, pp. 4927–4932.

[5] J. Kwiatkowski, D. Cockburn, and V. Duchaine, "Grasp stability assessment through the fusion of proprioception and tactile signals using convolutional neural networks," in *2017 IEEE/RSJ International Conference on Intelligent Robots and Systems (IROS)*, Sept 2017, pp. 286–292.

[6] L. Pinto and A. Gupta, "Supersizing self-supervision: Learning to grasp from 50k tries and 700 robot hours," in *2016 IEEE International Conference on Robotics and Automation (ICRA)*, May 2016, pp. 3406–3413.

[7] Y. Chebotar, K. Hausman, Z. Su, G. S. Sukhatme, and S. Schaal, "Self-supervised regrasping using spatio-temporal tactile features and reinforcement learning," in *2016 IEEE/RSJ International Conference on Intelligent Robots and Systems (IROS)*, Oct 2016, pp. 1960–1966.

[8] M. Li, K. Hang, D. Kragic, and A. Billard, "Dexterous grasping under shape uncertainty," *Robotics and Autonomous Systems*, vol. 75, pp. 352 – 364, 2016. [Online]. Available: http://www.sciencedirect.com/science/article/pii/S0921889015001967

[9] R. Calandra, A. Owens, D. Jayaraman, J. Lin, W. Yuan, J. Malik, E. H. Adelson, and S. Levine, "More than a feeling: Learning to grasp and regrasp using vision and touch," *CoRR*, vol. abs/1805.11085, 2018. [Online]. Available: http://arxiv.org/abs/1805.11085

[10] H. Kawasaki, T. Komatsu, K. Uchiyama, and T. Kurimoto, "Dexterous anthropomorphic robot hand with distributed tactile sensor: Gifu hand ii," in *IEEE SMC'99 Conference Proceedings. 1999 IEEE International Conference on Systems, Man, and Cybernetics (Cat. No.99CH37028)*, vol. 2, Oct 1999, pp. 782–787 vol.2.

[11] J. M. Romano, K. Hsiao, G. Niemeyer, S. Chitta, and K. J. Kuchenbecker, "Human-inspired robotic grasp control with tactile sensing," *IEEE Transactions on Robotics*, vol. 27, no. 6, pp. 1067–1079, Dec 2011.

[12] A. J. Spiers, M. V. Liarokapis, B. Calli, and A. M. Dollar, "Single-grasp object classification and feature extraction with simple robot hands and tactile sensors," *IEEE Transactions on Haptics*, vol. 9, no. 2, pp. 207–220, April 2016.

[13] M. Kaboli, A. D. L. R. T, R. Walker, and G. Cheng, "In-hand object recognition via texture properties with robotic hands, artificial skin, and novel tactile descriptors," in *2015 IEEE-RAS 15th International Conference on Humanoid Robots (Humanoids)*, Nov 2015, pp. 1155–1160.

[14] H. Soh and Y. Demiris, "Incrementally learning objects by touch: Online discriminative and generative models for tactile-based recognition," *IEEE Transactions on Haptics*, vol. 7, no. 4, pp. 512–525, Oct 2014.

[15] R. Li and E. H. Adelson, "Sensing and recognizing surface textures using a gelsight sensor," in *2013 IEEE Conference on Computer Vision and Pattern Recognition*, June 2013, pp. 1241–1247.

[16] B. Ward-Cherrier, N. Pestell, L. Cramphorn, B. Winstone, M. E. Giannaccini, J. Rossiter, and N. F. Lepora, "The tactip family: Soft optical tactile sensors with 3d-printed biomimetic morphologies," *Soft Robotics*, vol. 5, pp. 216–277, 2018.

[17] C. Chorley, C. Melhuish, T. Pipe, and J. Rossiter, "Development of a tactile sensor based on biologically inspired edge encoding," in *2009 International Conference on Advanced Robotics*, 2009, pp. 1–6.

[18] N. F. Lepora and B. Ward-Cherrier, "Superresolution with an optical tactile sensor," in *2015 IEEE/RSJ International Conference on Intelligent Robots and Systems (IROS)*, 2015, pp. 2686–2691.

[19] B. Ward-Cherrier, L. Cramphorn, and N. F. Lepora, "Tactile manipulation with a tacthumb integrated on the open-hand m2 gripper," *IEEE Robotics and Automation Letters*, vol. 1, no. 1, pp. 169–175, Jan 2016.

[20] B. Ward-Cherrier, N. Rojas, and N. F. Lepora, "Model-free precise in-hand manipulation with a 3d-printed tactile gripper," *IEEE Robotics and Automation Letters*, vol. 2, no. 4, pp. 2056–2063, 2017.

[21] "Shadow Robot Company agile grasper documentation," https://agile-grasper.readthedocs.io/en/latest/, accessed: 2018-09-07.

[22] L. Cramphorn, J. Lloyd, and N. F. Lepora, "Voronoi features for tactile sensing: Direct inference of pressure, shear, and contact locations," in *2018 IEEE International Conference on Robotics and Automation (ICRA)*, 2018.

[23] OpenAI, M. Andrychowicz, B. Baker, M. Chociej, R. Jowicz, B. McGrew, J. Pachocki, A. Petron, M. Plappert, G. Powell, A. Ray, J. Schneider, S. Sidor, J. Tobin, P. Welinder, L. Weng, and W. Zaremba, "Learning dexterous in-hand manipulation," *CoRR*, 2018. [Online]. Available: http://arxiv.org/abs/1808.00177